Remote Sensing of Environment 184 (2016) 302–315

Contents lists available at ScienceDirect

Remote Sensing of Environment

journal homepage: www.elsevier.com/locate/rse

Landslide susceptibility map refinement using PSInSAR data

Andrea Ciampalini *, Federico Raspini, Daniela Lagomarsino, Filippo Catani, Nicola Casagli

Department of Earth Sciences, University of Firenze, via La Pira 4, 50121 Firenze, Italy

ARTICLE INFO

Article history:
Received 3 February 2016
Received in revised form 23 June 2016
Accepted 14 July 2016
Available online xxxx

Keywords:
Landslide
Susceptibility
SAR interferometry
SqueeSAR
Sicily

ABSTRACT

Landslide susceptibility maps (LSM) are commonly used by local authorities for land use management and planning activities, representing a valuable tool used to support decision makers in urban and infrastructural planning. The accuracy of a landslide susceptibility map is affected by false negative and false positive errors which can decrease the reliability of this useful product. In particular, false negative errors, are generally worse in terms of social and economic losses with respect to the losses associated with false positives. In this paper, we present a new technique to improve the accuracy of landslide susceptibility maps using Permanent Scatterer Interferometric Synthetic Aperture Radar (PSInSAR) data. The proposed approach uses two different data sets acquired in ascending and descending geometry. The PS velocity measured along the line of sight is re-projected into a new velocity along the steepest slope direction ($\mathbf{V_{Slope}}$). Integration between the LSM and the ground deformation velocity map along the slope was performed using an empirical contingency matrix, which takes into account the average $\mathbf{V_{Slope}}$ and the susceptibility degree obtained using the Random Forests algorithm. The Results show that the susceptibility degree increased in 56.41 km^2 of the study area. The combination of PSInSAR data and the landslide susceptibility map (LSM) improved the prediction reliability of slow moving landslides, which particularly affect urbanized areas. The use of this procedure can be easily applied in different areas where PSI data sets are available. This approach will help planning and decision-making authorities produce reliable landslide susceptibility maps, correcting some of the LSM errors.

1. Introduction

Landslide susceptibility is defined as the likelihood of a landslide occurring in an area based on local terrain conditions (Brabb, 1984) and represents the degree to which an area can be affected by future slope failure (Rossi et al., 2010). From a quantitative point of view, landslide susceptibility is the relative probability of the spatial occurrence of slope failure, considering different geological, topographical and environmental conditions in a study area (Chung and Fabbri, 1999; Guzzetti et al., 2005, 2006). The temporal probability of a landslide is not included in susceptibility models. Several papers devoted to the concepts, principles, techniques and methods associated with landslide susceptibility have been published over the past 30 years (Carrara, 1983; Brabb, 1984; Hansen, 1984; Varnes and IAEG Commission on Landslides and Other Mass-Movements, 1984; van Westen, 1994; Soeters and van Westen, 1996; van Westen et al., 1997; Aleotti and Chowdhury, 1999; Chung and Fabbri, 1999; Guzzetti et al., 1999; Vandine et al., 2004; Catani et al., 2005; Crozier and Glade, 2005; Ermini et al., 2005; Guzzetti et al., 2006; Rossi et al., 2010; Catani et al., 2013; Jebur et al., 2014). Landslide susceptibility maps are essential for effective land use management and planning activities and are valuable tools that can support decision makers' urban and infrastructural plans. There is an increasing interest in producing helpful methodologies for local authorities who then choose the best management strategies, including minimizing impacts from land use activities in landslide-prone areas (Gorsevski et al., 2006). Landslide susceptibility maps can be produced using several methods and techniques available in the literature, often using geographic information systems (GIS) (van Westen et al., 2006; Chacon et al., 2006). Among the available methods to map landslide susceptibility, statistical- and landslide inventory-based probabilistic techniques (Carrara et al., 1995; Guzzetti et al., 1999; Chacon et al., 2006) can be used. These methods are generally used in combination. For example, landslide-conditioning parameter maps, bivariate statistical methods, multivariate statistical methods and machine learning techniques such as artificial neural networks and fuzzy logic approaches can be combined to create landslide susceptibility maps (Chacon et al., 2006; Lee et al., 2007). Landslide parameters (slope angle, lithology, aspect, elevation, etc.) have been combined using bivariate statistical methods (i.e., Yalcın, 2008; Regmi et al., 2010; Oh et al., 2010; Sterlacchini et al., 2011), multivariate statistical methods (i.e., Ohlmacher and Davis, 2003; Ayalew and Yamagishi, 2005; Duman et al., 2006; Kıncal et al., 2009; Van Den Eeckhaut et al., 2010; Rossi et al., 2010; Bai et al., 2010; Atkinson and Massari, 2011), machine learning methods (Catani et al., 2005; Ermini et al., 2005; Yesilnacar and Topal, 2005; Wu and Chen, 2009; Nefeslioglu et al.,

* Corresponding author.
E-mail address: andrea.ciampalini@unifi.it (A. Ciampalini).

http://dx.doi.org/10.1016/j.rse.2016.07.018

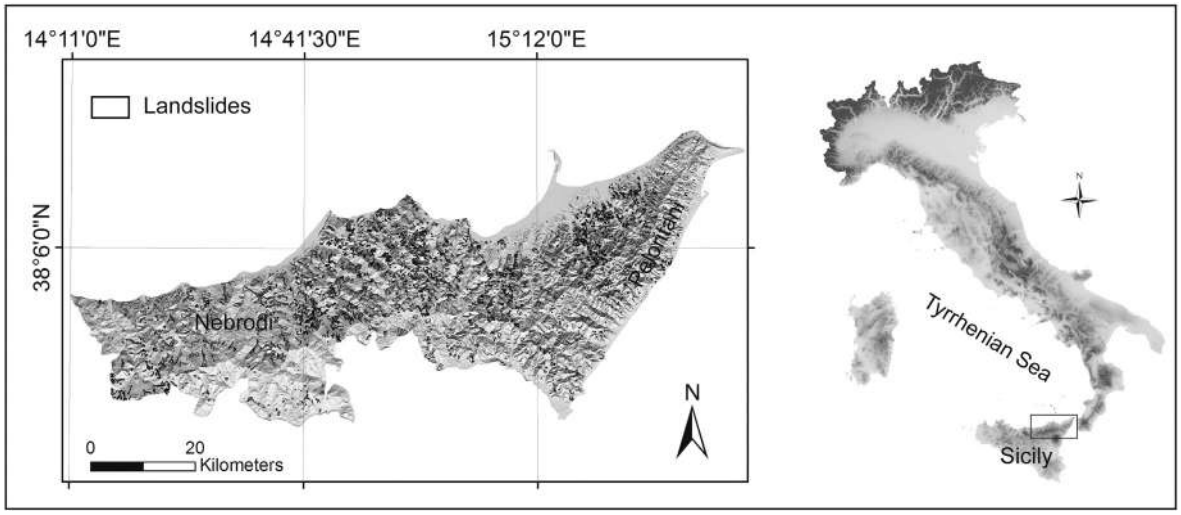

Fig. 1. Location of the study area, its morphology (from a 20 m resolution DEM) and the available landslide inventory map.

2010; Pradhan et al., 2010; Melchiorre et al., 2011), conditional probability or Bayesian methods (Catani et al., 2013) and landslide inventory-based probabilistic methods (Casagli et al., 2004; Lee, 2005; Lee and Pradhan, 2007; Akgun et al., 2008). The classification of a certain terrain affects its economic value. From an economic point of view, the value of a stable area will be higher than that of an unstable area. Thus, an appropriate susceptibility model must reduce the misclassification of terrains and minimize economic and non-economic costs. The techniques used to evaluate the accuracy of landslide susceptibility models generally do not include misclassification costs. This is a relevant problem in landslide susceptibility analysis. The most common errors in susceptibility models can be summarized into two different groups (Frattini et al., 2010):

Error Type I (false positive): terrains not affected by landslides are classified as unstable. Thus, that their economic value is incorrectly decreased by restricting to their use. In this case, the misclassification leads to a social cost equal to the loss of economic value of the terrain plus indirect costs related to the consequences of forcing landowners to move or acquire new land parcels.

Error Type II (false negative): terrains affected by ground deformation are classified as stable and incorrectly used without restrictions. In this case, the cost of the misclassification may be higher because of the underestimation of the possible losses of elements at risk (live, buildings, etc.) that can be involved in a landslide event. Compared to false positives, false negative errors are usually worse in terms of social and economic losses.

Reducing both error types is a priority in operational landslide risk management and a current issue. To achieve this goal Permanent Scatterer Interferometric Synthetic Aperture Radar (PSInSAR) data can be effectively used, especially in case studies of slow or very slow moving landslides (Ferretti et al., 2000, 2001). Ground displacement measurements can be obtained using the SqueeSAR technique (Ferretti et al., 2011) developed by Tele-Rilevamento Europa (T.R.E.). By combining a landslide susceptibility map with PSInSAR data, the degree of landslide susceptibility in those areas affected by ground deformation can be updated and corrected, reducing the number of false negatives and increasing the reliability of the landslide susceptibility map (Oliveira et al., 2015; Piacentini et al., 2015). This work focuses on the reduction of false negatives. It is not possible to correct false positives because ground deformation detection using PSInSAR is related to a precise time interval. Thus, a terrain susceptible to landslides can be stable in that period but remain prone to hillslope processes. In this paper, we test this approach in Messina Province (southern Italy), which is an area strongly affected by slow-moving landslides.

Table 1
Details of the available CSK SAR data from 2011 to 2012.

	Ascending	Descending
Temporal range	01/05/2011–03/05/2012	16/05/2011–02/05/2012
No. of images	51	64
No. of PS-DS	453,331	793,725
PS-DS/km^2	288.31	729.94
Mean $\mathbf{V_{Los}}$ (mm/year)	−0.49	−0.43
Min. $\mathbf{V_{Los}}$ (mm/year)	−78.90	−73.97
Max. $\mathbf{V_{Los}}$ (mm/year)	29.29	33.26
Stability threshold (mm/year)	±3.5	±4.5

2. Study area

Messina Province is located in the northeastern portion of Sicily Island (southern Italy, Fig. 1). It is part of the Sicilian fold-and-thrust orogenic belt formed during the Africa-Europe plate collision. NE Sicily is divided into three tectonic domains (Pavano et al., 2015): (i) the Peloritani Ridge, (ii) the Nebrodi-Peloritani Transition zone and (iii) the Nebrodi Mountains. The Peloritani Ridge is located along the eastern coast of Sicily (Ionian coast) and comprises a basement represented by Aspromonte and Mandanaci Units (Lentini et al., 2000). The basement is made up of high-grade crystalline rocks and low-grade metapelites (Pavano et al., 2015; Mineo et al., 2015). Along the coast, overlying metamorphic rocks, Late Miocene to Middle Pleistocene marine deposits crop out (Lentini et al., 2000; Del Ventisette et al., 2012). The Nebrodi-Peloritani Transition zone is represented by a narrow belt bounded by the Taormina Line (Ghisetti and Vezzani, 1982) to the southwest and by Tindari-Capo S. Alessio Alignment (Catalano et al., 1996) to the northeast. This area is characterized by the presence of epimetamorphic rocks, with a few relics of Mesozoic sedimentary succession. These lithologies are covered by well-developed Oligo-Miocene terrigenous deposits. The western sector is constituted by the Nebrodi Mountains, which represent the culmination of Paleogene Tethyan

Table 2
Statistics of the PS data set after the projection along the steepest slope (ST = stability threshold; max $\mathbf{V_{Slope}}$, mean $\mathbf{V_{Slope}}$ and ST are expressed in mm/year).

Geometry	No. of PS/DS	PS-DS/km^2	Discarded PS	Max $\mathbf{V_{Slope}}$	Mean $\mathbf{V_{Slope}}$	ST
Ascending	100,870	82	352,461			
Descending	182,609	148.46	611,116			
Asc + Desc	283,479	230	965,577	−168.4	−6.91	0 to −7

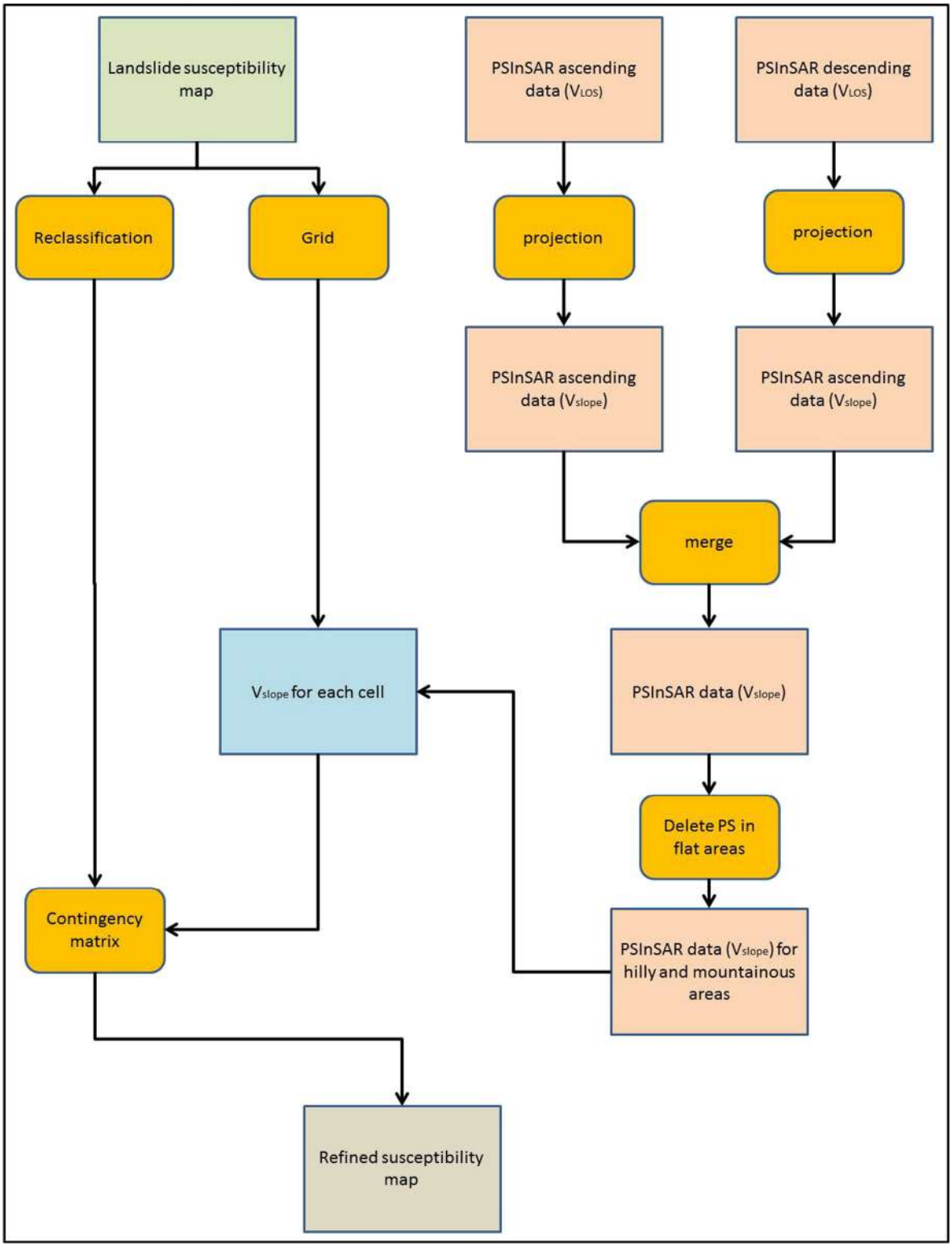

Fig. 2. Flow chart illustrating the adopted methodology.

accretionary wedge terrains. The morphology of the study area is strongly influenced by this geological framework. Both coastal segments (Ionian and Tyrrhenian) are characterized by the presence of coastal mountain ridges (Peloritani and Nebrodi) with steep slopes, narrow valleys perpendicular to the coast and high relief energies (Ciampalini et al., 2015a).

The coastal V-shaped river basins are reduced watercourse networks with regular and parallel paths that significantly transport solid materials during the wet season (September–April). Along the Tyrrhenian coast, small alluvial plains are present. The rivers crossing both mountain chains are called "fiumare". They are usually straight, with steep courses and gravel beds (Raspini et al., 2015). The climate of the region is a typical Mediterranean climate, characterized by prominent seasonality; therefore, the river regime is irregular (Ciampalini et al., 2015a). Exceptional rainfall events combined with the presence of steep slopes on fractured rocks represent the main landslide-triggering

Table 3
Contingency matrix applied to the LSM considering the average $\mathbf{V_{Slope}}$ in each cell.

		V_{Slope}(mm/year)			
		0–7	7–14	14–21	> 21
Suscept. degree	1	0	+1	+2	+3
	2	0	0	+1	+2
	3	0	0	0	+1
	4	0	0	0	0

factor (Ardizzone et al., 2012). In the case of exceptional rainfall, debris flows are the most common hillslope processes that occur in the Peloritani ridge, whereas rotational, translational and complex landslides are more common within both the Nebrodi Mountains and the Nebrodi-Peloritani Transition zone (Del Ventisette et al., 2012; Bardi et al., 2014). Between autumn 2009 and winter 2010, several exceptional rainfall events occurred in Messina Province. During October 2009, the Ionian coast was affected by >600 landslides (Ardizzone et al., 2012; Cama et al., 2015). Several small settlements were considerably damaged, 37 people died (Ciampalini et al., 2015a) and 122 people were injured. At the beginning of 2010, prolonged and widespread rainfall caused hundreds of complex landslides along the Tyrrhenian coast (Del Ventisette et al., 2013; Bianchini et al., 2014; Ciampalini et al., 2014; Bardi et al., 2014; Raspini et al., 2015) where buildings and infrastructures located in several municipalities were damaged. Overall, 8978 hillslope processes are mapped in the available Landslide Inventory Map (LIM, Piano di Assetto Idrogeologico, 2012, PAI) of Messina Province. They consist of: 1259 rock falls or topples (14.02%), 508 rapid flows (5.66%), 1531 slides (17.05%), 1546 complex slides (17.22%), 355 flows (3.95%), 962 superficial instability events (10.72%), 764 creep or solifluctions (8.51%) and 2053 rapid erosion events (22.87%). From a lithological viewpoint, the lithologies involved in the hillslope processes vary depending on the area. For example, within the Peloritani Mountains, most landslides involve rocks belonging to the crystalline basement and its Meso-Cenozoic sedimentary cover (Messina et al., 2004). On the contrary, the hillslope processes in the Nebrodi Mountains mostly involve Oligocene to Pleistocene deposits because Flysch and wedge-top deposits extensively crop out in this area (Di Paolo et al., 2014).

3. Methodology

3.1. Landslide Susceptibility Map

The landslide susceptibility map (LSM) of Messina Province was produced by implementing a Random Forests (RF) algorithm in Matlab (Catani et al., 2013). This technique is a machine learning algorithm for non-parametric multivariate classification that was developed by Breiman (2001) based on classification trees, providing high classification accuracy without overfitting (Diaz-Uriarte and de Andres, 2006). RF is commonly used to classify remote sensing data (Duro et al., 2012; Lawrence et al., 2006; Watts et al., 2009; Chen et al., 2014), but it has been rarely used in landslide susceptibility evaluation (Catani et al., 2013; Segoni et al., 2014; Triglia et al., 2015). The variables considered for the LSM of Messina Province were extracted from the following available maps and data layers: a geological map (scale 1:50,000), a land cover map (2000 Corine Land Cover, scale 1:100,000), the existing landslide inventory map (PAI – Piano di Assetto Idrogeologico, 2012) and DEM-derived products (DEM from the Istituto Geografico Militare, IGM). To avoid subjectivity in the choice of explanatory variables, several parameters were considered among the DEM-derived products: Aspect, Planar Curvature, Profile Curvature, Curvature s.s., Elevation, Flow Accumulation, Topographic Wetness Index (TWI), Log Flow Accumulation and Slope. The choice of parameters depends on the map unit resolution (MUR) (Catani et al., 2013). Among the possible parameters, we used those suggested for a map unit resolution of 100 m. Using this MUR, the expected Area Under the Curve (AUC) value is 0.81. A training set was created by randomly selecting 10% of the landslide database. Using this percentage, the expected AUC value is 0.88 (Catani et al., 2013). Furthermore, the standard deviation and variance were calculated for each numerical variable categorical variable, respectively, using a moving window of 100 by 100 m (Lagomarsino et al., 2014). The DEM had a 20 by 20 m spatial resolution. In the LSM, the average value inside a 100 by 100 m cell was calculated. Each pixel was classified using four susceptibility classes: (i) low to null (0–0.3); (ii) moderate (0.3–0.55); (iii) high (0.55–0.75) and (iv) very high (0.75–1). Although the choice of cutoff values for the definition of susceptibility classes is arbitrary

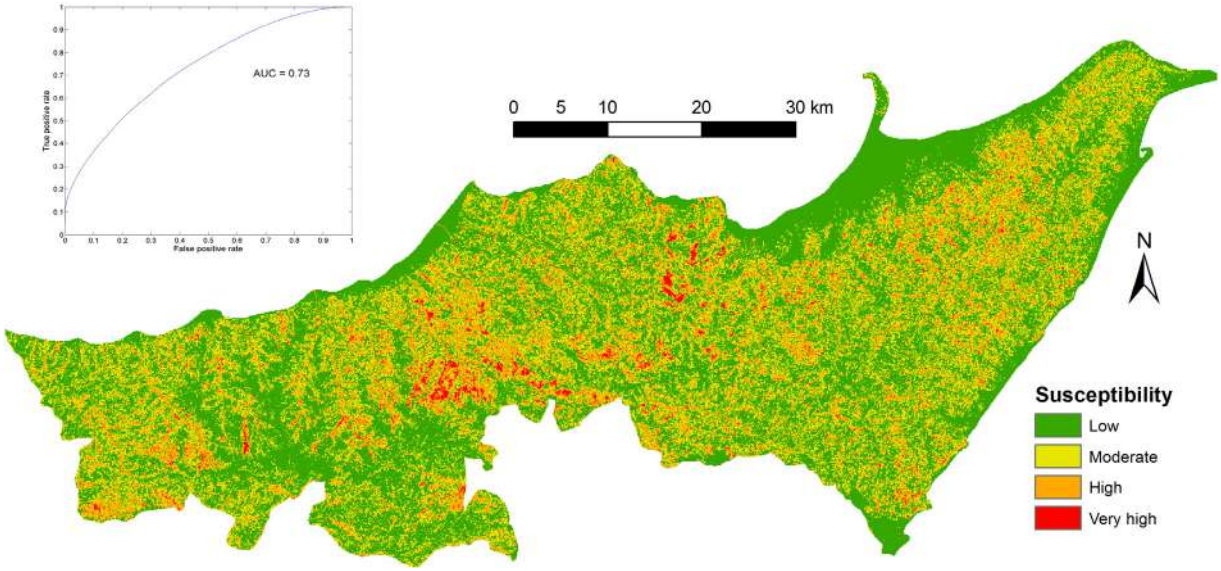

Fig. 3. Landslide susceptibility map of Messina Province and the related ROC curve.

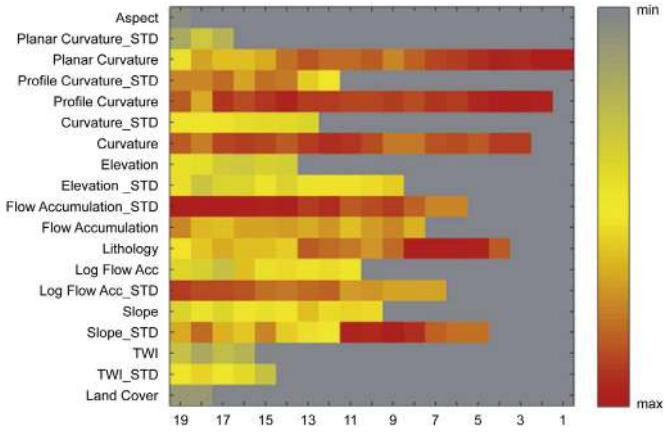

Fig. 4. Example plot illustrating the variation of parameter relative importance (expressed as rank using the colour ramp on the right) with parameter space (no. of parameters used LCV#).

(Frattini et al., 2010), the adopted ranges have been determined based on the best ROC (Receiver Operating Characteristic) curve.

3.2. PSInSAR

Permanent Scatterer Interferometry is an advanced multi-interferometric SAR technique used in ground deformation studies and can measure ground displacement with millimetre accuracy (Ferretti et al., 2000, 2001; Hanssen, 2005; Crosetto et al., 2010). PSInSAR techniques are extensively used to study soil subsidence (Herrera et al., 2010; Raspini et al., 2014), earthquakes (Tronin, 2006; Sousa et al., 2010; Lagios et al., 2012), volcanic activity (Peltier et al., 2010; Branca et al., 2014; Parker et al., 2014) and landslides (Bianchini et al., 2012; Ciampalini et al., 2014; Bardi et al., 2014). The PSInSAR method relies on the analysis of a backscattered signal from co-registered, multi temporal synthetic aperture radar (SAR) images (at least 15) to identify highly reflective ground elements, which are stable from an electromagnetic point of view, called Permanent Scatterers (PS) (Ferretti et al., 2000, 2001; Werner et al., 2003). The SqueeSAR™ algorithm (Ferretti et al., 2011) is an evolution of the PSInSAR technique that measures ground displacements using both PS and the Distributed Scatterers (DS), which correspond to homogeneous areas spread across a group of pixels in a SAR image (e.g., rangeland, pasture, shrubs and bare soils). The SqueeSAR technique considerably increases the point target density compared to that of the traditional PSInSAR technique, especially in sparsely vegetated landscapes (Bellotti et al., 2014; Notti et al., 2014). Both the PSInSAR and SqueeSAR™ techniques can measure the movements of each PS/DS along the satellite Line Of Sight (LOS) with respect to an assumed stable point (Massironi et al., 2009). Point targets correspond to anthropogenic (e.g., buildings and metallic structures) or natural objects (e.g., rock outcrops) with stable radar signatures (Ferretti et al., 2000). Thus, urbanized areas have high numbers of PS. On the contrary, the SqueeSAR approach is more useful in rural, agricultural and rocky areas. Ground displacement measurements were obtained for a part of Messina Province using the SqueeSAR™ technique (Ciampalini et al., 2015a) by processing SAR images acquired by X-band COSMO-SkyMed (CSK) in Stripmap mode (40 × 40 km in the range and azimuth directions and 3 × 3 m ground resolution) in both ascending and descending geometry (Table 1).

The PS/DS located outside Messina Province were removed from the total PS/DS in each data set. For each PS/DS, ground deformation velocities are measured in the direction of the satellite Line of Sight (LOS) and do not correspond to the real velocity, which occurs in three dimensions (Cascini et al., 2009). To compare and handle both PSI data sets acquired in ascending and descending geometry, a post-processing step is needed. By projecting the $\mathbf{V_{Los}}$ velocity (mean yearly velocities measured along the LOS) vectors in the direction of the steepest slope, in combination with a DEM, the two data sets can be combined into a single data set, in which each PS/DS is linked to its $\mathbf{V_{Slope}}$ velocity, which is now an along-slope vector. The most reliable displacement can be measured in the direction of the local maximum slope gradient, which is considered the most probable direction of real movement associated with a potential slope failure (Cascini et al., 2010; Notti et al., 2010; Plank et al., 2012; Bianchini et al., 2013; Herrera et al., 2013; Ciampalini et al., 2016). The projection of $\mathbf{V_{Los}}$ along the steepest slope was performed using the formula proposed by Bianchini et al. (2013) and Notti et al. (2014). This approach requires knowledge of the following factors: (i) the slope and aspect derived from the DEM; and (ii) the satellite acquisition parameters (i.e., the azimuth, the incidence angle, the directional cosines: nlos, hlos, and elos of the LOS). This method is useful when SAR images are acquired by different satellite sensors (with different LOSs) and/or different acquisition orbits (i.e., ascending and descending). It can easily interpret and compare displacements projected in a common direction (steepest slope direction). This procedure significantly reduces the PS/DS population because all PS/DS with positive velocities (i.e., upslope directions, reflecting terrain uplift) were discarded (Notti et al., 2010) (Table 2). Furthermore, because PSInSAR also detects terrain subsidence, PS/DS located in areas characterized by slope gradients lower than 5° were discarded. In total, 283,479 PS/DS were available after the discarding phase over an area of 1230 km^2, resulting in a final density of 230 PS-DS/km^2.

The PS/DS density reduction was offset by the more reliable evaluation of ground deformation obtained using $\mathbf{V_{Slope}}$ instead of $\mathbf{V_{Los}}$ and by combining different PSI data sets acquired at the same time. Moreover, the final PS/DS density is still acceptable. For example, 96 PS/km^2 is considered high density in geological studies at the regional scale (Meisina et al., 2008). The PSI data sets are now comparable and they can be merged into a single PSI data set, where each PS/DS is linked to its related $\mathbf{V_{Slope}}$.

3.3. Integration

To combine the LSM and PSI data set, the former was reclassified by assigning a numerical value to each classes as follows: low to null susceptibility = 1; moderate susceptibility = 2; high susceptibility = 3; very high susceptibility = 4. Furthermore, a grid with a 100 m resolution was created. A single cell in the grid corresponds to a single cell in the LSM. The integration relies on coupling the degree of susceptibility in each cell (100 by 100 m) with an average $\mathbf{V_{Slope}}$ value based on the PS/DS velocity in the area (Fig. 2).

The aim of the integration procedure is to increase the susceptibility degree of those cells characterized by ground deformation, reducing missed alerts. On the contrary, cells characterized by high susceptibility degrees that are stable according to SAR interferometry were not modified. In fact, the absence of detectable movements in the PSInSAR time frame does not necessarily imply that the susceptible area is actually stable. Based on the data sets, susceptibility updating was applied according to an empirical contingency matrix (Table 3). The matrix takes into account the average $\mathbf{V_{Slope}}$ module and the susceptibility degree obtained using the Random Forests algorithm.

The $\mathbf{V_{Slope}}$ intervals were determined based on the standard deviation (σ = 7 mm/year) of $\mathbf{V_{Slope}}$ for the whole PSI data set after merging the ascending and descending data sets. The matrix in Table 3 shows the correction factors for each considered case. The velocity intervals were determined to increase the susceptibility degree from level 1 to 4. For example, an area characterized by a susceptibility degree of 1 will increase by 1 degree if its $\mathbf{V_{Slope}}$ falls within 1 σ to 2 σ of the stability threshold (7–14 in this case), 2 degrees if the $\mathbf{V_{Slope}}$ is between 2 σ and 3 σ and so on. The higher the ground deformation velocity, the higher the susceptibility degree. A cell characterized by the maximum susceptibility degree cannot increase further. To determine how

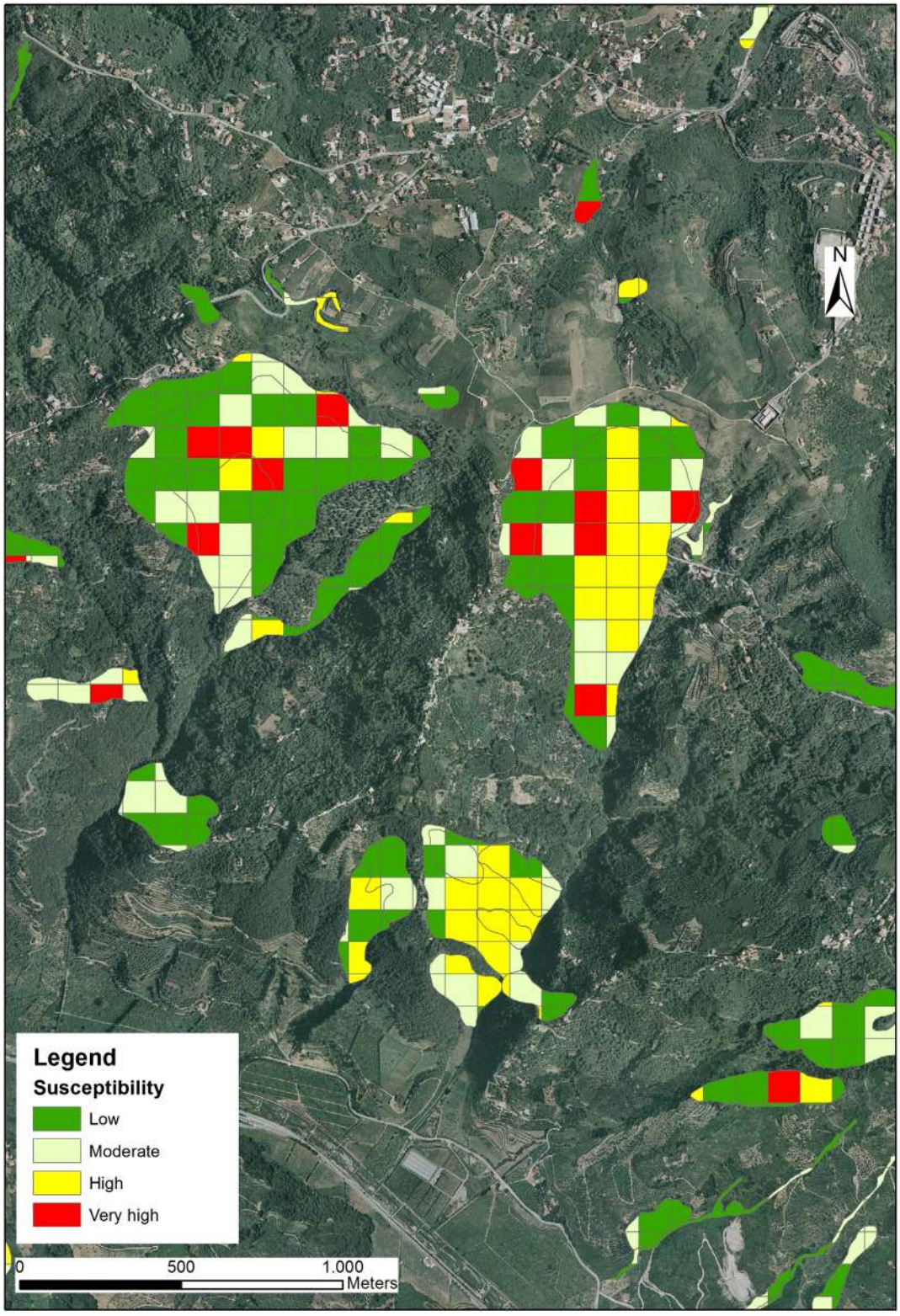

Fig. 5. Example of false negatives (cells classified in the low susceptibility class but included within a landslide boundary).

may PS/DS could be used to update the susceptibility degree of a 100×100 m cell, the areas of all the landslides included in the available LIM were considered. The smallest landslide was 25 m^2. Thus, we used the average velocity based on at least four PS/DS to update the susceptibility degree of a single cell. Cells containing less than three PS/DS were not updated.

4. Results

4.1. The LSM of the Messina Province

The LSM of Messina Province (Fig. 3) was classified using four different classes: (i) low to null susceptibility; (ii) moderate susceptibility;

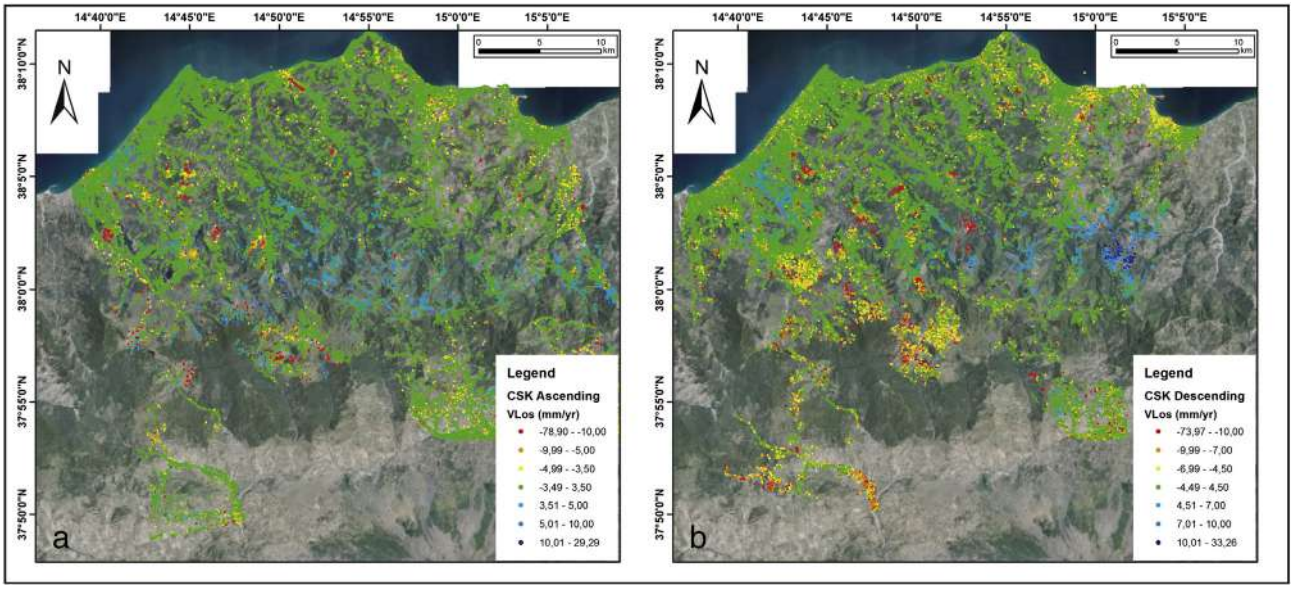

Fig. 6. Ground deformation velocity maps obtained using the V_{Los} ascending data set (a) and V_{Los} descending data set (b).

(iii) high susceptibility and (iv) very high susceptibility. The performance of the model was evaluated by building an ROC curve (Deleo, 1993; Beguería, 2006; Gorsevski et al., 2006). The AUC value of 0.73 represents a fairly good result for an LSM at the regional scale (Catani et al., 2013). This result is lower than the expected value (between 0.81 and 0.88), considering the selected MUR and the size of the training set. Because the target of the proposed approach is the refinement of the LSM, the accuracy of the produced LSM, with an AUC value of 0.73, can be improved.

The LSM suggests that a consistent part of Messina Province is characterized by a moderate to very high landslide susceptibility. In particular, a brief statistical analysis shows that the 51.52% of Messina Province

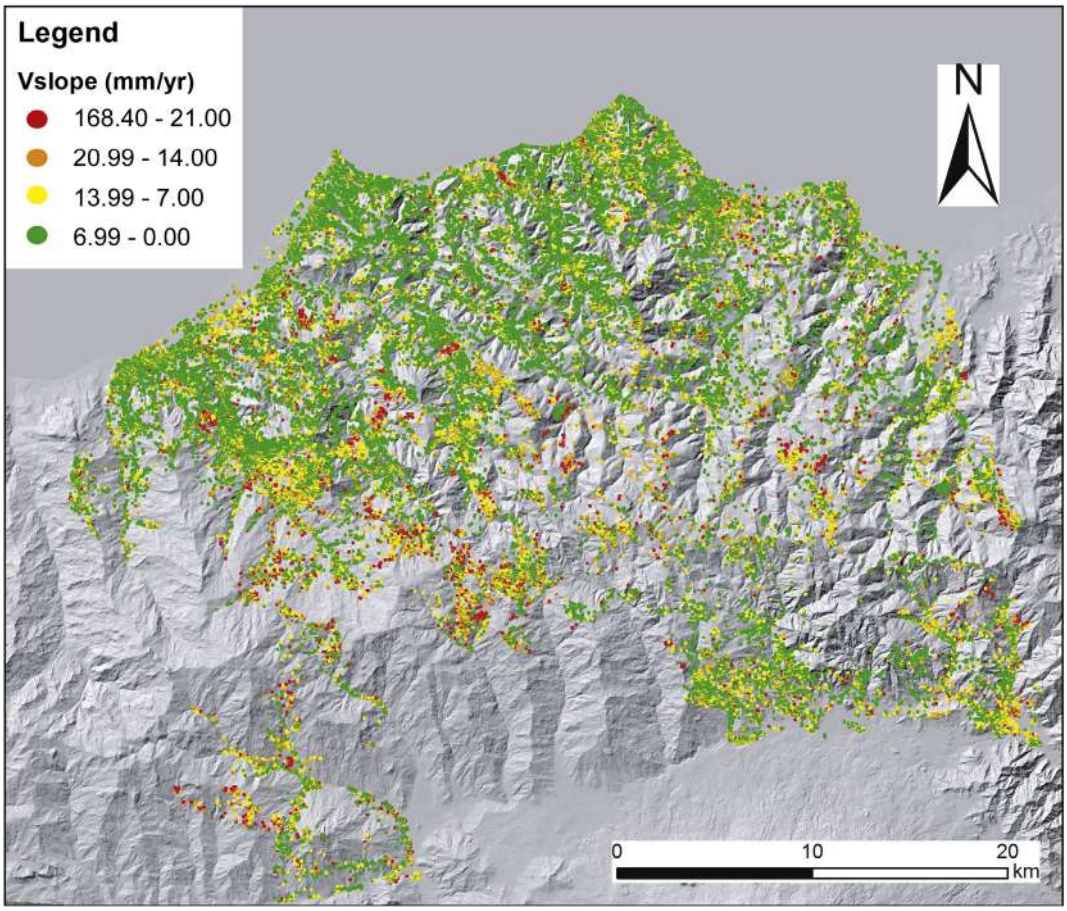

Fig. 7. Ground deformation velocity map obtained for the investigated area using the V_{Slope} velocities.

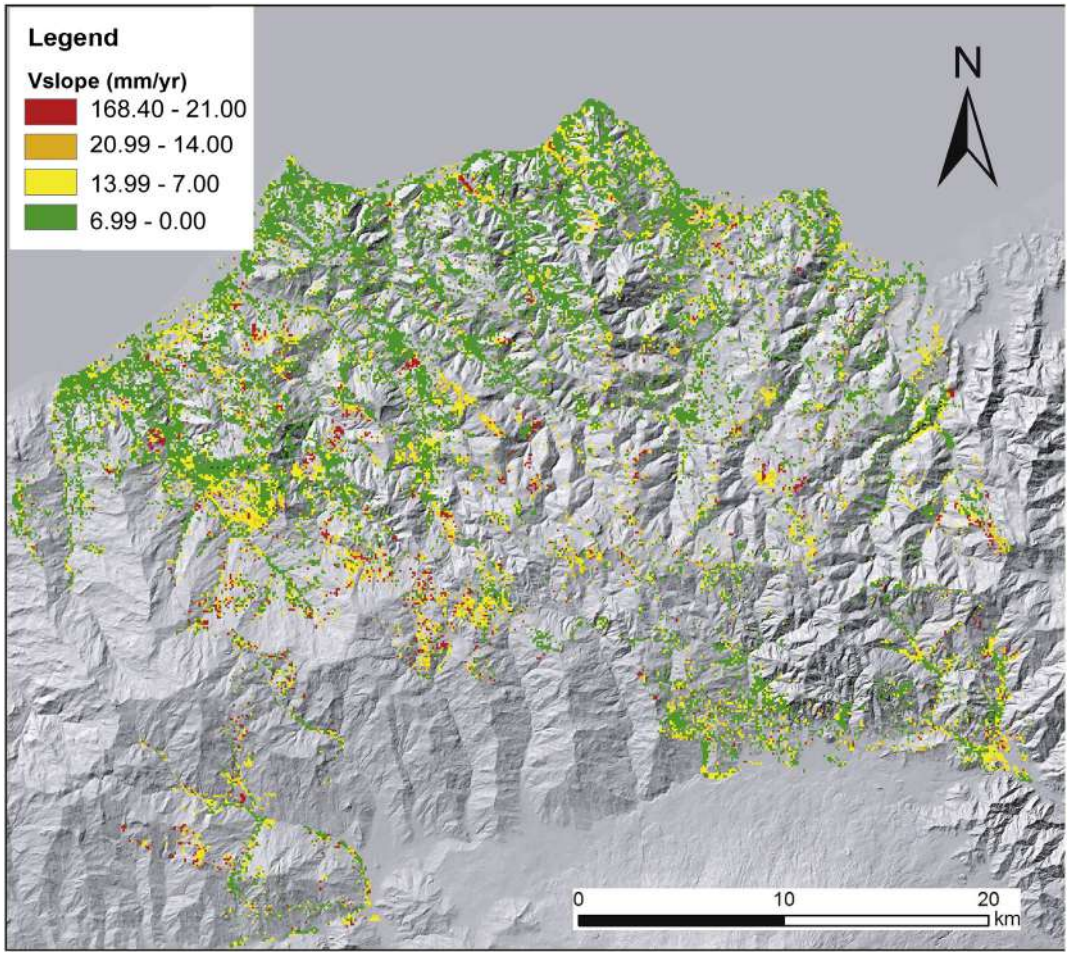

Fig. 8. Ground deformation velocity map of each cell in the study area considering the average $\mathbf{V_{Slope}}$ velocity of the PS/DS included in the single cell.

is classified as low susceptibility, 29.10% as moderate, 17.31% as high and 2.07% as very high. Most of the areas affected by low susceptibility are located along the coast, corresponding to narrow coastal alluvial plains. If we consider the study area covered by the SAR data (see Section 4.2), the percentages are as follows: 45.61% low to null susceptibility, 30.51% moderate susceptibility, 20.62% high susceptibility and 3.26% very high susceptibility. The ranking and significance of landslide conditioning variables (LCV) can be used to identify the predisposing landslide factors in the province (Fig. 4).

The most influential LCVs are mainly related to Slope Curvature, Flow Accumulation and Slope Angle, suggesting that the landslide susceptibility of the area is driven by erosion and runoff processes (Zeverbergen and Thorne, 1987). Furthermore, the importance of Slope Curvature is enhanced in this area because it represents a signature of landslide presence, as it is potentially related to the typical concave to convex pattern of the landslide profile (Catani et al., 2010). Plan Curvature and Flow Accumulation rankings suggest that water flux and soil saturation (Catani et al., 2005; Xu et al., 2013) may affect the

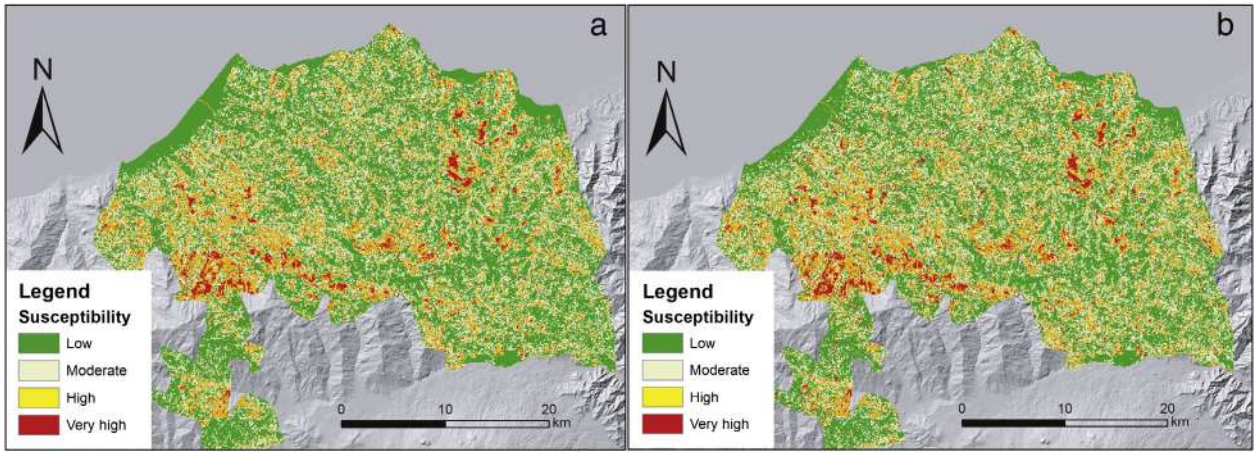

Fig. 9. Comparison between the LSM obtained by applying the RF algorithm (a) and the new LSM after the application of the correction matrix (b).

Table 4
Overview of the results obtained by comparing the old and new LSMs.

Suscept. degree	Old LSM		New LSM		Increase	
Class	No. cells	%	No. cells	%	Class	No. cells
1	54,052	45.61	48,849	42.06	0	112,856
2	36,151	30.51	37,895	31.98	+1	3776
3	24,435	20.62	25,441	21.47	+2	1236
4	3859	3.26	5320	4.49	+3	629

landslide susceptibility of Messina Province more than other factors. The importance of slope angle is expected, as it usually represents one of the most important predisposing factors (Guzzetti et al., 1999). In particular, its standard deviation can be considered an indicator of the potential energy associated with erosion and mass wasting (Catani et al., 2013) or a measure of relief energy. To evaluate the accuracy of the LSM, the numbers of cells classified into the lowest susceptibility class included within landslide polygons of the landslide inventory map were counted (Fig. 5).

These cells can be considered false negatives that are part of landslides but classified as not susceptible to mass movements. In this case, the percentage of false negatives is 25.23%. This percentage must be added to the possible false negatives corresponding to areas that are not mapped in the LIM but are affected by slope instability phenomena. This result stresses the importance of defining a new method to compensate for such errors.

4.2. PSInSAR

A PSInSAR analysis was only performed in the central part of Messina Province covered by the satellite acquisitions (Fig. 6). A brief visual inspection of the ground deformation velocity maps obtained through the $\mathbf{V_{Los}}$ velocity confirmed that the study area is particularly affected by ground deformation phenomena (landslides and coastal subsidence). This area is 1230 km^2 and was used to test the procedure by combining PSI data and the LSM to refine the latter.

The ground deformation velocity map depicting the $\mathbf{V_{Slope}}$ velocity is reported in Fig. 7. The stability threshold (0–7.00 mm/year) was chosen considering the standard deviation of the velocity of the PSI data set (ascending and descending). In this area, 65% of the PS/DS population is characterized by stability. The obtained ground deformation velocity map highlights the presence of several clusters of moving PS/DS that do not always correspond to landslides mapped in the available LIM.

4.3. Integration

The first result of the integration procedure is the production of a new ground deformation velocity map where $\mathbf{V_{Slope}}$ is no longer related to a single PS/DS but to a 100 by 100 m cell (Fig. 8). Notably, cells in which PS/DS are absent cannot be classified. In this case, the average $\mathbf{V_{Slope}}$ can be measured based on 28,279 (23.85%) of the total 118,497 cells. The number of cells in which the average ground deformation velocity can be measured is strongly affected by the vegetation cover, which reduces the usefulness of the SqueeSAR™ technique. After producing the ground deformation velocity map for each cell, the correction matrix can be applied to refine the landslide susceptibility map.

The new LSM (Fig. 9) is characterized by a decrease in the percentage of the low susceptibility class. In particular, in the new map, class 1 (low to null susceptibility) includes 42.06% of the total number of cells, class 2 (moderate susceptibility) includes 31.98%, class 3 (high susceptibility) includes 21.47% and class 4 includes 4.49% (Table 4).

To evaluate the magnitude of the difference between the original LSM and the new LSM, the difference between them was calculated based on the values of the susceptibility degree of each cell (Fig. 10). The difference suggests that 5641 cells increase their susceptibility degree (56.41 km^2): 3776 cells (37.76 km^2) show an increase of 1 degree, 1236 (12.36 km^2) increase by 2 degrees and 629 (6.29 km^2) increase by 3 degrees (Table 4).

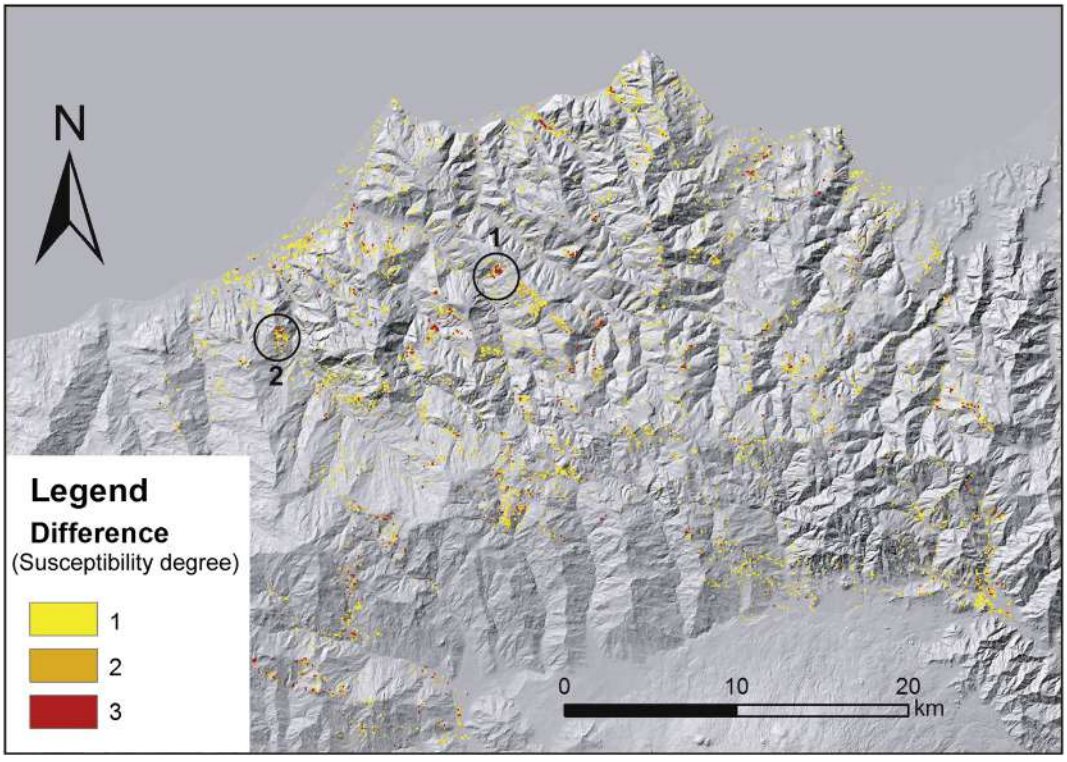

Fig. 10. Difference between the original LSM and the new LSM considering the susceptibility degree of each cell. Circle 1 corresponds to Castell'Umberto village and circle 2 corresponds to Militello Rosmarino village.

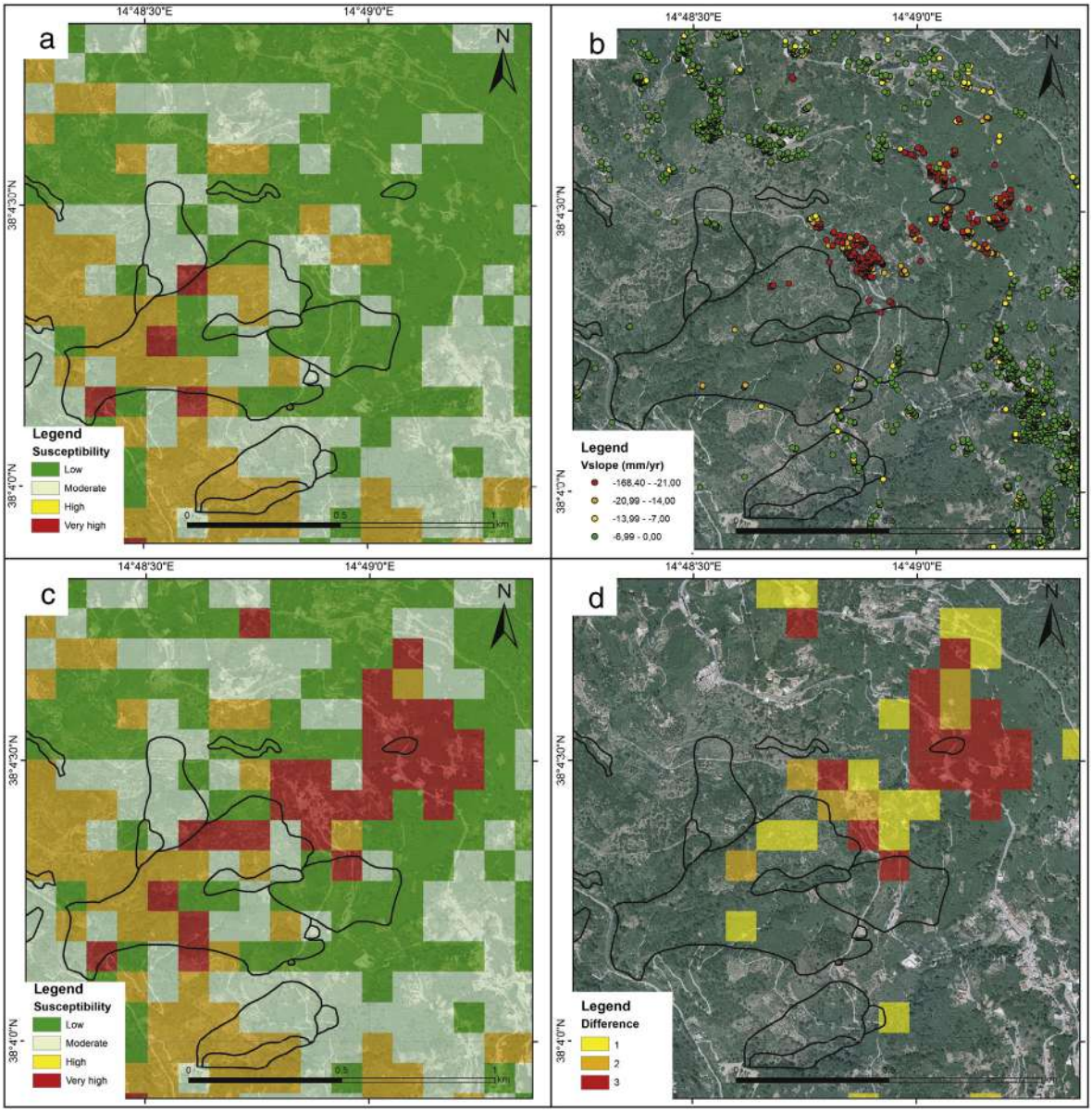

Fig. 11. (a) Original LSM of the Castell'Umberto municipality area; (b) $\mathbf{V_{Slope}}$ ground deformation velocity map; (c) new LSM obtained after the application of the correction matrix; (d) difference between the original LSM and the new LSM.

4.3.1. Results of specific case studies

We will briefly discuss the details of two specific cases in which the map in Fig. 10 highlights the existence of areas where very severe negative errors were noted, exhibiting a 3-degree increase in susceptibility after PSInSAR refinement. The first case is represented by the area of the Castell'Umberto municipality. Castell'Umberto is a small town located at 660 m a.s.l., and it is strongly affected by landslide. In particular, the town was rebuilt in 1865 after a large landslide almost destroyed its historical section. In the available landslide inventory map, several landslides are mapped along the slope of Castell'Umberto (Fig. 11).

In detail, two complex landslides were reported in an area where several residential buildings and strategic roads are located. Most of the LSM cells located in the area affected by the largest landslide show a high and very high susceptibility, as predicted using the Random Forests algorithm (Fig. 11a). On the upper part of the slope, where no landslides are mapped, the susceptibility degree is lower. Most of the cells are characterized by a low to null susceptibility degree. However, the PSI data set highlights a different scenario (Fig. 11b). The PS/DS velocity field confirms that the biggest complex landslide is still active and shows $\mathbf{V_{Slope}}$ values higher than 21 mm/year. Additionally, the velocity field shows that most of the slope above the landslide boundary is clearly affected by ground deformation that is not correctly predicted by the RF method. In this case, use of the correction matrix to update the LSM can be beneficially applied. The new LSM (Fig. 11c) assigns the highest susceptibility degree to a wider part of the slope considering those areas affected by ground deformation highlighted in the PSI map. After this step, updating the landslide inventory map and extending the boundary of the biggest landslide is recommended.

The area close to Militello Rosmarino was chosen as the second case (Fig. 12). Militello Rosmarino is a small village located within the Nebrodi Mountains and in the Rosmarino valley, at an elevation of 450 a.s.l. Its southeastern slope is strongly affected by hillslope processes. In particular, two large rock falls involving the hill where the village is located and several complex landslides to the south were recently detected (Raspini et al., 2015). This area was chosen to test the proposed approach because in the available LIM (PAI) few landslides are mapped.

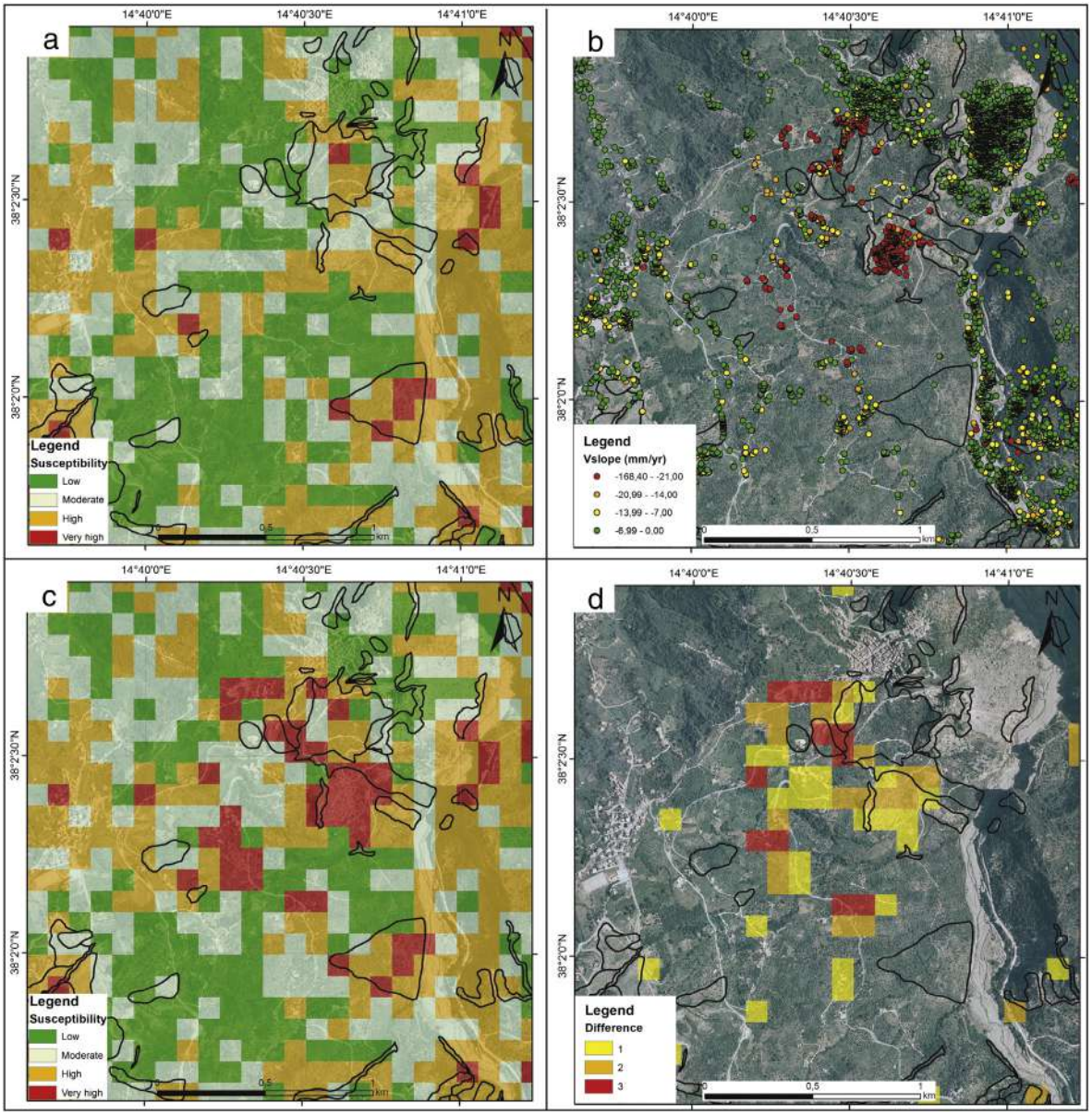

Fig. 12. (a) Original LSM of Militello Rosmarino municipality area; (b) $\mathbf{V_{Slope}}$ ground deformation velocity map; (c) new LSM obtained after the application of the correction matrix; (d) difference between the original LSM and the new LSM.

On the contrary, PSI data show the presence of spreading ground deformation on several parts of the slope located southeast of Militello Rosmarino. Furthermore, in this area, a geomorphological field survey was performed to validate PSI data and update the LIM (Raspini et al., 2015).

PSI data allowed the detection of ground deformation phenomena located southeast of Militello Rosmarino, which were confirmed through a geomorphological field survey that mapped several large complex landslides. These landslides were not included in the old LIM. In fact, the susceptibility degree evaluated using the Random Forest Algorithm (Fig. 12a) underestimates the real susceptibility of the area, which is characterized by high ground deformation velocities (Fig. 12b). The map of the difference between the classic LSM and the updated LSM (Fig. 12c) shows that several landslides are not mapped in the LIM used to create the LSM (Fig. 12d). In this case, the negative errors in the LSM are likely due to the missing objects in the original LIM used to calibrate the RF technique and not due to the susceptibility procedure itself. Nonetheless, the use of the refinement matrix in Table 3 is very important when applied to update the LIM or when used in post-processing to correct LSM classification. A new LIM (Raspini et al., 2015) has been created based on the new evidence. This updated product can be used to produce an updated LSM at the local scale considering some previously undetected phenomena (Fig. 13).

5. Discussion

The comparison between the original LSM obtained through a classic approach and the refined LSM created using SqueeSAR™ data shows that the methodology described in this work may lead to an improvement in the susceptibility ranking of a portion of the study area (about a quarter). This limitation is due to the intrinsic limitation of the SAR technique, which systematically fails in the case of vegetated areas. Wide and mountainous areas such as Messina Province are characterized by the presence of diffuse vegetation. To improve the PS/DS detection, L-band SAR sensors can be used because their wavelength (30–15 cm) is more suitable to investigate densely vegetated areas. The use of L-band data reduces temporal decorrelation effects induced by vegetation coverage (Strozzi et al., 2005) improving the penetration

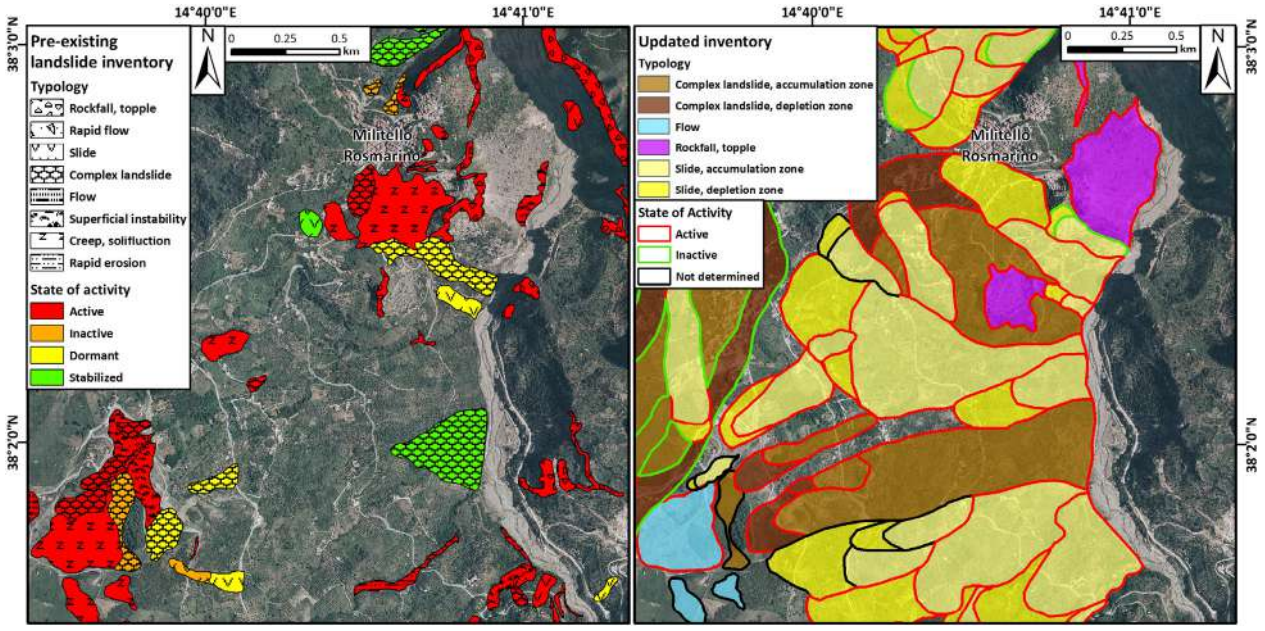

Fig. 13. Comparison between the available LIM (PAI) and the new LIM updated using both PSI data and a field survey.

capacity of the radar signal. The component of the decorrelation due to the vegetation in the L-band SAR images pairs is lower with respect to C-band and X-band components because of its higher signal wavelength and lower signal frequency (Wei and Sandwell, 2010).

Another important limitation of this approach is represented by the displacement rate of the investigated phenomena. The applicability of the PSI techniques is limited to extremely slow and very slow movements (vel. < 16 mm/year and 16 mm/year ≤ vel. < 1.6 m/year, respectively). This limitation, which is related to the radar wavelength, the revisiting time of the platform and the spatial density of measurement points prevent the use of PSI data when updating LSMs considering all hillslope processes, especially fast phenomena (e.g., rock falls, topples, and debris flows).

Although SAR images acquired in the X-band exhibit greater acquisition difficulties in vegetated areas with respect to those in L-band or C-band, their reduced revisiting times in the same area, shorter λ values, and reduced temporal decorrelation allow the detection of ground motions characterized by higher velocities.

The use of X-band images processed using the SqueeSAR approach lead to a significant improvement in the PS/DS density. Considering the loss of information (in terms of PS/DS density) after the merger of ascending and the descending data sets, a high PS/DS density in the original data is recommended. However, LSM is a fundamental tool in landscape management and can be used to evaluate the risks for people and infrastructures threatened by landslides. Therefore, the need for a very accurate LSM is of primary importance in urbanized areas where PSI data exhibit their maximum density. Generally, PS/DS are used to update the available landslide inventory map (LIM). After the LIM is updated, it can be used to produce a more reliable LSM. This approach is often time consuming, especially in broad areas where each landslide must be checked, added, enlarged or modified based on the PS/DS distribution and velocity. To produce an accurate LSM using SqueeSAR™ data, the described methodology is faster and highlights areas where clusters of moving PS/DS suggest that new landslides should be added to the LIM or that a boundary of a preexisting landslide requires modification. Both the landslide susceptibility map and the ground deformation velocity map can be used in different ways to forecast landslide occurrence in a selected area. Combining them may improve the reliability associated with predicting these types of phenomena, particularly for slow moving landslides. The high standard deviation, which affects the detected ground deformation velocity of the used data set, is due to the short period of acquisition (1 year), and it should be reduced by increasing the number of processed images. Although the PSI data set is a dynamic data set, when compared to the parameters used for the LSM, it is still a sort of picture of the ground deformation acquired in a specific time interval that can change over time. To update the LSM using PSI data and reduce the standard deviation of the velocity, we suggest that a set of SAR images acquired over the previous two years is used or that the PSI data set is continuously updated. The latter can be an expensive option, but the launch of the new European satellites (Sentinel-1) may considerably reduce the cost.

6. Conclusion

In this paper, a new approach is presented to improve the accuracy of landslide susceptibility maps using PSI data. The methodology aims to reduce the number of false negatives (terrains affected by ground deformation but classified as stable). The importance of the reduction of false negative is due to threats to people and infrastructure located in areas affected by hillslope phenomena. These areas must be considered in LSMs which can be used to plan remediation actions and urban growth.

An LSM of Messina Province (Sicily, Italy) with a 100 by 100 m cell resolution was produced using a Random Forests (RF) algorithm in Matlab considering several static parameters. The accuracy of the resulting map was evaluated using the ROC curve. The method produced a fairly good AUC value (0.73), suggesting that the LSM accuracy van be improved. An estimation of false negatives was performed considering cells classified as stable and located inside landslide boundaries.

Two PSI X-band data sets (ascending and descending) acquired between 2011 and 2012 were merged after projecting of the PS/DS velocity along the steepest slope. The new ground deformation velocity map was used to calculate the mean ground deformation velocity of each cell in the LSM.

A contingency matrix based on both the susceptibility classification and the ground deformation velocity map was created. This matrix was used to increase the susceptibility degrees of cells characterized by a low susceptibility degree but high ground deformation velocity detected by the PSI data.

The new LSM shows a decrease in the areas classified in the low to null susceptibility class. In particular, the susceptibility degree increased in 112.82 km^2 of 1230 km^2.

The use of this procedure can be easily applied in different areas where PSI data sets are available. This approach will help planning and decision-making authorities produce reliable landslide susceptibility maps, especially in urbanized areas. Additionally, the approach can also be used to detect areas that require updated landslide inventory maps.

Acknowledgements

The research leading to these results received funding from the Italian Civil Protection Department (Project SAR.net 2015). The authors also extend their gratitude to three anonymous reviewers for their suggestions, which markedly improved the manuscript.

References

Akgun, A., Dag, S., Bulut, F., 2008. Landslide susceptibility mapping for a landslide-prone area (Findikli, NE of Turkey) by likelihood frequency ratio and weighted linear combination models. Environ. Geol. 54, 1127–1143.

Aleotti, P., Chowdhury, R., 1999. Landslide hazard assessment: summary review and new perspectives. Bull. Eng. Geol. Environ. 58, 21–44.

Ardizzone, F., Basile, G., Cardinali, M., Casagli, N., Del Conte, S., Del Ventisette, C., Fiorucci, F., Garfagnoli, F., Gigli, G., Guzzetti, F., Iovine, G., Mondini, A.C., Moretti, S., Panebianco, M., Raspini, F., Reichembach, P., Rossi, M., Tanteri, L., Terranova, O., 2012. Landslide inventory map for the Briga and the Giampilieri catchments, NE Sicily, Italy. Journal of Maps 8 (2), 176–180.

Atkinson, P.M., Massari, R., 2011. Autologistic modelling of susceptibility to landsliding in the Central Apennines, Italy. Geomorphology 130, 55–64.

Ayalew, L., Yamagishi, H., 2005. The application of GIS-based logistic regression for landslide susceptibility mapping in the Kakuda-Yahiko Mountains, Central Japan. Geomorphology 65, 15–31.

Bai, S.B., Wang, J., Lü, G.N., Zhou, P.G., Hou, S.S., Xu, S.N., 2010. GIS-based logistic regression for landslide susceptibility mapping of the Zhongxian segment in the Three Gorges area, China. Geomorphology 115, 23–31.

Bardi, F., Frodella, W., Ciampalini, A., Bianchini, S., Del Ventisette, C., Gigli, G., Fanti, R., Moretti, S., Basile, G., Casagli, N., 2014. Integration between ground based and satellite SAR data in landslide mapping: the San Fratello case study. Geomorphology 223, 45–60.

Beguería, S., 2006. Validation and evaluation of predictive models in hazards assessment and risk management. Nat. Hazards 37, 315–329.

Bellotti, F., Bianchi, M., Colombo, D., Ferretti, A., Tamburini, A., 2014. Advanced InSAR techniques to support landslide monitoring. In: Pardo-Igúzquiza, E., Guardiola-Albert, C., Heredia, J., Moreno-Merino, L., Durán, J.J., Vargas-Guzmán, J.A. (Eds.), Mathematics of Planet Earth, Lecture Notes in Earth System Sciences. Springer, Berlin Heidelberg, pp. 287–290.

Bianchini, S., Cigna, F., Righini, G., Proietti, C., Casagli, N., 2012. Landslide hotspot mapping by means of persistent scatterer interferometry. Environ. Earth Sci. 67 (4), 1155–1172.

Bianchini, S., Herrera, G., Notti, D., Garcìa-Moreno, I., Mora, O., Moretti, S., 2013. Landslide activity maps generation by means of Persistent Scatterer Interferometry. Remote Sens. 5 (12), 6198–6222.

Bianchini, S., Ciampalini, A., Raspini, F., Bardi, F., Di Traglia, F., Moretti, S., Casagli, N., 2014. Multi-temporal evaluation of landslide movements and impacts on buildings in San Fratello (Italy) by means of C-band and X-band PSI data. Pure Appl. Geophys. 172, 3043–3065.

Brabb, E.E., 1984. Innovative approaches to landslide hazard mapping. Proceedings 4th International Symposium on Landslides, Toronto vol. 1, pp. 307–324.

Branca, S., De Guidi, G., Lanzafame, G., Monaco, C., 2014. Holocene vertical deformation along the coastal sector of Mt. Etna volcano (eastern Sicily, Italy): implications on the time-space constrains of the volcano lateral sliding. J. Geodyn. 82, 194–203.

Breiman, L., 2001. Random forests. Mach. Learn. 45, 5–32.

Cama, M., Lombardo, L., Conoscenti, C., Agnesi, V., Rotigliano, E., 2015. Predicting storm-triggered debris flow events: application to the 2009 Ionian Peloritan disater (Sicily, Italy). Nat. Hazards Earth Syst. Sci. 15, 1785–1806.

Carrara, A., 1983. A multivariate model for landslide hazard evaluation. Math. Geol. 15, 403–426.

Carrara, A., Cardinali, M., Guzzetti, F., Reichenbach, P., 1995. GIS-based techniques for mapping landslide hazard. http://deis158.deis.unibo.it.

Casagli, N., Catani, F., Puglisi, C., Delmonaco, G., Ermini, L., Margottini, C., 2004. An inventory-based approach to landslide susceptibility assessment and its application to the Virginio River Basin, Italy. Environ. Eng. Geosci. 10 (3), 203–216.

Cascini, L., Fornaro, G., Peduto, D., 2009. Analysis at medium scale of low-resolution DInSAR data in slow-moving landslide-affected areas. ISPRS J. Photogram. Rem. Sens. 64 (6), 598–611.

Cascini, L., Fornaro, G., Peduto, D., 2010. Advanced low- and full-resolution DInSAR map generation for slow-moving landslide analysis at different scales. Eng. Geol. 112 (1–4), 29–42.

Catalano, S., Di Stefano, A., Vinci, G., 1996. Tettonica e sedimentazione nell'Oligocene-Miocene lungo l'allineamento Raccuia-Novara di Sicilia-Capo S. Alessio nei Monti Peloritani (Sicilia Nord-Orientale). Mem. Soc. Geol. It. 51, 165–177.

Catani, F., Casagli, N., Ermini, L., Righini, G., Menduni, G., 2005. Landslide hazard and risk mapping at catchment scale in the Arno River Basin. Landslides 2 (329–342), 2005.

Catani, F., Segoni, S., Falorni, G., 2010. An empirical geomorphology-based approach to the spatial prediction of soil thickness at catchment scale. Water Resour. Res. 46 (1–15), 2010.

Catani, F., Lagomarsino, D., Segoni, S., Tofani, V., 2013. Landslide susceptibility estimation by random forests techninque: sensitivity and scaling issues. Nat. Hazards Earth Syst. Sci. 13, 2815–2831.

Chacon, J., Irigaray, C., Fernandez, T., El Hamdouni, R., 2006. Engineering geology maps: landslides and geographical information systems. Bull. Eng. Geol. Environ. 65, 341–411.

Chen, W., Li, X., Wang, Y., Chen, G., Liu, S., 2014. Forested landslide detection using LiDAR data and the random forests algorithm: a case study of the Three Gorges, China. Remote Sens. Environ. 152, 291–301.

Chung, C.-J.F., Fabbri, A.G., 1999. Probabilistic prediction models for landslide hazard mapping. Photogramm. Eng. Remote. Sens. 65, 1389–1399.

Ciampalini, A., Bardi, F., Bianchini, S., Frodella, W., Del Ventisette, C., Moretti, S., Casagli, N., 2014. Analysis of building deformation in landslide area using multisensor PSInSAR™ technique. Int. J. Appl. Earth Obs. Geoinf. 33, 166–180.

Ciampalini, A., Raspini, F., Bianchini, S., Frodella, W., Bardi, F., Lagomarsino, D., Di Traglia, F., Moretti, S., Proietti, C., Pagliara, P., Onori, R., Corazza, A., Duro, A., Basile, G., Casagli, N., 2015a. Remote sensing as tool for development of landslide geodatabase: the case of the Messina Province (Italy) geodatabase. Geomorphology 249, 103–118.

Ciampalini, A., Raspini, F., Frodella, W., Bardi, F., Bianchini, S., Moretti, S., 2016. The effectiveness of high-resolution LiDAR data combined with PSInSAR data in landslide study. Landslides 13, 399–410.

Crosetto, M., Monserrat, O., Iglesias, R., Crippa, B., 2010. Persistent scatterer interferometry: potential, limits and initial C- and X-band comparison. Photogramm. Eng. Remote. Sens. 76 (9), 1061–1069.

Crozier, M.J., Glade, T., 2005. Landslide hazard and risk: issues, concepts and approach. In: Glade, T., Anderson, M.G., Crozier, M.J. (Eds.), Landslide Risk Assessment. In John Wiley, Chichester, pp. 1–40.

Del Ventisette, C., Garfagnoli, F., Ciampalini, A., Battistini, A., Gigli, G., Moretti, N., Casagli, N., 2012. An integrated approach to the study of catastrophic debris-flows: geological hazard and human influence. Nat. Hazards Earth Syst. Sci. 12, 2907–2922.

Del Ventisette, C., Ciampalini, A., Manunta, M., Calò, F., Paglia, L., Ardizzone, F., Mondini, A.C., Reichembach, P., Mateos, R.M., Bianchini, S., Garcia, I., Füsi, B., Deak, Z.V., Radi, K., Graniczny, M., Kowalski, Z., Piatkowska, A., Przylucka, M., Retzo, H., Strozzi, T., Colombo, D., Mora, O., Sanches, F., Herrera, G., Moretti, S., Casagli, S., Guzzetti, F., 2013. Exploitation of large archives of ERS and ENVISAT C-band SAR data to characterize ground deformations. Remote Sens. 5 (8), 3896–3917.

Deleo, J.M., 1993. Receiver operating characteristic laboratory (ROCLAB): software for developing decision strategies that account for uncertainty. Proceedings of the Second International Symposium on Uncertainty Modelling and Analysis. Computer Society Press, College Park, pp. 318–325.

Di Paolo, L., Olivetti, V., Corrado, S., Aldega, L., Balestrieri, M.L., Maniscalco, R., 2014. Detecting the stepwise propagation of the Eastern Sicily thrust belt (Italy): insight from thermal and thermocronological constraints. Terra Nova 26, 363–371.

Diaz-Uriarte, R., de Andres, S.A., 2006. Gene selection and classification of microarray data using random forest. BMC Bioinformatics 7, 3.

Duman, T.Y., Can, T., Gokceoglu, C., Nefeslioglu, H.A., Sonmez, H., 2006. Application of logistic regression for landslide susceptibility zoning of Cekmece Area, Istanbul, Turkey. Environ. Geol. 51, 241–256.

Duro, D.C., Franklin, S.E., Dube, M.G., 2012. Multi-scale object-based image analysis and feature selection of multi-sensor earth observation imagery using random forests. Int. J. Remote Sens. 33, 4502–4526.

Ermini, L., Catani, F., Casagli, N., 2005. Artificial Neural Networks applied to landslide susceptibility assessment. Geomorphology 66, 327–343.

Ferretti, A., Prati, C., Rocca, F., 2000. Non-linear subsidence rate estimation using permanent scatterers in differential SAR interferometry. IEEE Trans. Geosci. Remote Sens. 38 (5), 2202–2212.

Ferretti, A., Prati, C., Rocca, F., 2001. Permanent scatterers in SAR interferometry. IEEE Trans. Geosci. Remote Sens. 39 (1), 8–20.

Ferretti, A., Fumagalli, A., Novali, F., Prati, C., Rocca, F., Rucci, A., 2011. A new algorithm for processing interferometric data-stacks: SqueeSAR. IEEE Transaction on Geoscience and remote Sensing. 49 (9), 3460–3470.

Frattini, P., Crosta, G., Carrara, A., 2010. Techniques for evaluating the performance of landslide susceptibility models. Eng. Geol. 111, 62–72.

Ghisetti, F., Vezzani, L., 1982. The recent deformation mechanisms of the Calabrian Arc. Earth Ev. Sc. 3, 197–206.

Gorsevski, P.V., Gessler, P.E., Foltz, R.B., Elliot, W.J., 2006. Spatial prediction of landslide hazard using logistic regression and ROC analysis. Trans. GIS 10, 395–415.

Guzzetti, F., Carrara, A., Cardinali, M., Reichenbach, P., 1999. Landslide hazard evaluation: a review of current techniques and their application in a multi-scale study, Central Italy. Geomorphology 31, 181–216.

Guzzetti, F., Reichenbach, P., Cardinali, M., Galli, M., Ardizzone, F., 2005. Probabilistic landslide hazard assessment at the basin scale. Geomorphology 72, 272–299.

Guzzetti, F., Galli, M., Reichenbach, P., Ardizzone, F., Cardinali, M., 2006. Landslide hazard assessment in the Collazzone area, Umbria, central Italy. Nat. Hazards Earth Syst. Sci. 6, 115–131.

Hansen, A., 1984. Landslide hazard analysis. In: Brunsden, D., Prior, D.B. (Eds.), Slope Instability. Wiley & Sons, New York, pp. 523–602.

Hanssen, R.S., 2005. Satellite radar interferometry for deformation monitoring: a priori assessment of feasibility and accuracy. Int. J. Appl. Earth Obs. Geoinf. 6, 253–260.

Herrera, G., Tómas, R., Monells, D., Centolanza, G., Mallorquí, J.J., Vicente, F., Navarro, V.D., Lopez-Sanchez, J.M., Sanabria, M., Cano, M., Mulas, J., 2010. Analysis of subsidence using TerraSAR-X data: Murcia case study. Eng. Geol. 116, 284–295.

Herrera, G., Gutiérrez, F., García-Davalillo, J.C., Guerrero, J., Notti, D., Galve, J.P., Fernández-Merodo, J.A., Cooksley, G., 2013. Multi-sensor advanced DInSAR monitoring of very slow landslides: the Tena Valley case study (Central Spanish Pyrenees). Remote Sens. Environ. 128, 31–43.

Jebur, M.N., Pradhan, B., Tehrany, M.S., 2014. Optimization of landslide conditioning factors using very high-resolution airborne laser scanning (LiDAR) data at catchment scale. Remote Sens. Environ. 152, 150–165.

Kıncal, C., Akgun, A., Koca, M.Y., 2009. Landslide susceptibility assessment in the Izmir (West Anatolia, Turkey) city center and its near vicinity by the logistic regression method. Environ. Earth Sci. 59, 745–756.

Lagios, E., Papadimitriou, P., Novali, F., Sakkas, V., Fumagalli, A., Vlachou, K., Del Conte, S., 2012. Combined seismicity pattern analysis, DGPS and PSInSAR studies in the broader area of Cephalonia (Greece). Tectonophysics 524-525, 43–58.

Lagomarsino, D., Segoni, S., Fanti, R., Catani, F., Casagli, N., 2014. Regional scale landslide susceptibility mapping in Emilia Romagna (Italy) as a tool for early warning. Landslide Science for a safer Geoenvironment 443–449.

Lawrence, R.L., Wood, S.D., Sheley, R.L., 2006. Mapping invasive plants using hyperspectral imagery and Breiman Cutler classifications (Random Forest). Remote Sens. Environ. 100, 356–362.

Lee, S., 2005. Application of logistic regression model and its validation for landslide susceptibility mapping using GIS and remote sensing data. Int. J. Remote Sens. 26, 1477–1491.

Lee, S., Pradhan, B., 2007. Landslide hazard mapping at Selangor, Malaysia using frequency ratio and logistic regression models. Landslides 4, 33–41.

Lee, S., Ryu, J.H., Kim, L.S., 2007. Landslide susceptibility analysis and its verification using likelihood ratio, logistic regression, and artificial neuralnetwork models: case study of Youngin, Korea. Landslides 4, 327–338.

Lentini, F., Catalano, S., Carbone, S., 2000. Carta Geologica della Provincia di Messina. SELCA, Firenze (2000).

Massironi, M., Zampieri, D., Bianchi, M., Schiavo, A., Franceschini, A., 2009. Use of PSInSAR ™ data to infer active tectonics: clues on the differential uplift across the Giudicarie belt (Central-Eastern Alps, Italy). Tectonophysics 476, 297–303.

Meisina, C., Zucca, F., Notti, D., Colombo, A., Cucchi, A., Savio, G., Giannico, C., Bianchi, M., 2008. Geological interpretation of PSInSAR data at regional scale. Sensors 8, 7469–7492.

Melchiorre, C., Castellanos, E.A., van Westen, C.J., Matteucci, M., 2011. Evaluation of prediction capability, robustness and sensitivity in non linear landslide susceptibility models, Guantanamo, Cuba. Comput. Geosci. 37, 410–425.

Messina, A., Somma, R., Careri, G., Carbone, G., Macaone, E., 2004. Peloritani continental crust composition (southern Italy): geological and petrochemical evidences. Boll. Soc. Geol. It. 123, 405–441.

Mineo, S., Pappalardo, G., Rapisarda, F., Cubito, A., Di Maria, G., 2015. Integrated geostructural, seismic and infrared thermography surveys for the study of an unstable rock slope in the Peloritani Chain (NE Sicily). Eng. Geol. 195, 225–235.

Nefeslioglu, H.A., Sezer, E., Gokceoglu, C., Bozkır, A.S., Duman, T.Y., 2010. Assessment of landslide susceptibility by decision trees in the metropolitan area of Istanbul, Turkey. Math. Probl. Eng. 2010 (Article ID: 901095).

Notti, D., Davalillo, J.C., Herrera, G., Mora, O., 2010. Assessment of the performance of X-band satellite radar data for landslide mapping and monitoring: Upper Tena Valley case study. Nat. Hazards Earth Syst. Sci. 10, 1865–1875.

Notti, D., Herrera, G., Bianchini, S., Meisina, C., García-Davalillo, J.C., Zucca, F., 2014. A methodology for improving landslide PSI data analysis. Int. J. Remote Sens. 35, 2186–2214.

Oh, H.J., Lee, S., Soedradjat, G.M., 2010. Quantitative landslide susceptibility mapping at Pemalang area, Indonesia. Environ. Earth Sci. 60, 1317–1328.

Ohlmacher, C.G., Davis, C.J., 2003. Using multiple regression and GIS technology to predict landslide hazard in northeast Kansas, USA. Eng. Geol. 69, 331–343.

Oliveira, S.C., Zêzere, J.L., Catalão, J., Nico, G., 2015. The contribution of PSInSAR interferometry to landslide hazard in weak rock-dominated areas. Landslides 12 (4), 703–771.

PAI, 2012. Piano Stralcio di Bacino per l'Assetto Idrogeologico AdB Regione Sicilia. http://www.sitr.regione.sicilia.it/pai.

Parker, A.L., Biggs, J., Lu, Z., 2014. Investigationg long-term subsidence at Medicine Lake Volcano, CA, using multitemporal InSAR. Geophys. J. Int. 199, 844–859.

Pavano, F., Romagnoli, G., Tortorici, G., Catalano, S., 2015. Active tectonics along the Nebrodi-Peloritani boundary in northeastern Sicily (Southern Italy). Tectonophysics 659, 1–11.

Peltier, A., Bianchi, M., Kaminski, E., Komorowski, J.-C., Rucci, A., Staudacher, T., 2010. PSInSAR as a new tool to monitor pre-eruptive volcano ground deformation: validation using GPS measurements on Piton de la Fournaise. Geophys. Res. Lett. 37, L12301. http://dx.doi.org/10.1029/2010GL043846.

Piacentini, D., Devoto, S., Mantovani, M., Pasuto, A., Prampolini, M., Soldati, M., 2015. Landslide susceptibility modeling assisted by Persistent Scatterers Interferometry (PSI): an example from the northwestern coast of Malta. Nat. Hazards 78 (1), 681–697.

Plank, S., Singer, J., Minet, C., Thuro, K., 2012. Pre-survey suitability evaluation of the differential synthetic aperture radar interferometry method for landslide monitoring. Int. J. Remote Sens. 33 (20), 6623–6637.

Pradhan, B., Lee, S., Buchroithner, M.F., 2010. A GIS-based back-propagation neural network model and its cross-application and validation for landslide susceptibility analyses. Comput. Environ. Urban. Syst. 34, 216–235.

Raspini, F., Loupasakis, K., Rozos, D., Adam, N., Moretti, S., 2014. Ground subsidence phenomena in the Delta municipality region (Northern Greece): geotechnical modeling and validation with Persistent Scatterer Interferometry. Int. J. App. Earth Ob. Geo. Inf. 28, 78–89.

Raspini, F., Ciampalini, A., Bianchini, S., Bardi, F., Di Traglia, F., Basile, G., Moretti, S., 2015. Updated landslide inventory of the area between the Furiano and Rosmarino creeks (Sicily, Italy). Journal of Maps http://dx.doi.org/10.1080/17445647.2015.1114975.

Regmi, N.R., Giardino, J.R., Vitek, J.D., 2010. Modeling susceptibility to landslides using the weight of evidence approach: Western Colorado, USA. Geomorphology 115, 172–187.

Rossi, M., Guzzetti, F., Reichenbach, P., Mondini, A.C., Peruccacci, S., 2010. Optimal landslide susceptibility zonation based on multiple forecasts. Geomorphology 114, 129–142.

Segoni, S., Lagomarsino, D., Fanti, R., Moretti, S., Casagli, N., 2014. Integration of rainfall thresholds and susceptibility maps in the Emilia Romagna (Italy) regional-scale landslide warning system. Landslides http://dx.doi.org/10.1007/s10346-014-0502-0.

Soeters, R., van Westen, C.J., 1996. Slope instability recognition, analysis and zonation. In: Turner, A.K., Schuster, R.L. (Eds.), Landslide Investigation and Mitigation: National Research Council, Transportation Research Board Special Report vol. 247, pp. 129–177.

Sousa, J.J., Ruiz, A.M., Hanssen, R.F., Bastos, L., Gil, A.J., Galindo-Zaldívar, J., Sanz de Galdeano, C., 2010. PS-InSAR processing methodologies in the detection of field surface deformation – study of the Granada basin (Central Betic Cordilleras, southern Spain). J. Geodyn. 49, 181–189.

Sterlacchini, S., Ballabio, C., Blahut, J., Masetti, M., Sorichetta, A., 2011. Spatial agreement of predicted patterns in landslide susceptibility maps. Geomorphology 125, 51–61.

Strozzi, T., Farina, P., Corsini, A., Ambrosi, C., Thüring, M., Zilger, J., Wiesmann, A., Wegmüller, U., Werner, C., 2005. Survey and monitoring of landslide displacements by means of L-band satellite SAR interferometry. Landslides 2, 193201.

Triglia, A., Iadanza, C., Esposito, C., Scarascia-Mugnozza, G., 2015. Comparison of Logistic Regression and Random Forests techniques for shallow landslide susceptibility assessment in Giampilieri (NE Sicily, Italy). Geomorphology http://dx.doi.org/10.1016/j.geomorph.2015.06.001.

Tronin, A.A., 2006. Remote sensing and earthquakes: a review. Physics and Chemistry of the Earth, Parts A/B/C 31, 138–142.

Van Den Eeckhaut, M., Marre, A., Poesen, J., 2010. Comparison of two landslide susceptibility assessments in the Champagne–Ardenne region (France). Geomorphology 115, 141–155.

Vandine, D.F., Moore, G., Wise, M., Vanbuskirk, C., Gerath, R., 2004. Chapter 3 — technical terms and methods. In: Wise, M., Moore, G., VanDine, D. (Eds.), Landslide Risk Case Studies in Forest Development Planning and Operations: B.C., Ministry of Forests, Forest Science Program, Abstract of Land Management Handbook vol. 56, pp. 13–26.

Varnes, D.J., IAEG Commission on Landslides and Other Mass-Movements, 1984m. Landslide Hazard Zonation: A Review of Principles and Practice. The UNESCO Press, Paris (63 pp).

Watts, J.D., Lawrence, R.L., Miller, P.R., Montagne, C., 2009. Monitoring of cropland practices for carbon sequestration purposes in north central Montana by Landsat remote sensing. Remote Sens. Environ. 113, 1843–1852.

Wei, M., Sandwell, D.T., 2010. Decorrelation of L-band and C-band interferometry over vegetated areas in California. IEEE Trans. Geosc. Remote Sens. 48, 2942–2952.

Werner, C., Wegmuller, U., Strozzi, T., Wiesmann, A., 2003. Interferometric Point Target Analysis for deformation mapping. Proceedings of IGARSS 2003, Toulouse (Francia).

van Westen, C.J., 1994. GIS in landslide hazard zonation: a review with examples from the Colombian Andes. In: Price, M.F., Heywood, D.I. (Eds.), Mountain Environments & Geographical Information Systems. Taylor and Francis, London, pp. 135–165.

van Westen, C.J., Rengers, N., Terlien, M.T.J., Soeters, R., 1997. Prediction of the occurrence of slope instability phenomenal through GIS-based hazard zonation. Geol. Rundsch. 86, 404–414.

van Westen, C.J., van Asch, T.W.J., Soeters, R., 2006. Landslide hazard and risk zonation—why is it still so difficult? Bull. Eng. Geol. Environ. 65, 167–184.

Wu, C.H., Chen, S.C., 2009. Determining landslide susceptibility in Central Taiwan from rainfall and six site factors using the analytical hierarchy process method. Geomorphology 112, 190–204.

Xu, W., Yu, W., Jing, S., Zhang, G., Huang, J., 2013. Debris flow susceptibility assessment by GIS and information value model in a large-scale region, Sichuan Province (China). Nat. Hazards 65, 1379–1392.

Yalcın, A., 2008. GIS-based landslide susceptibility mapping using analytical hierarchy process and bivariate statistics in Ardesen (Turkey): comparisons of results and confirmations. Catena 1, 1–12.

Yesilnacar, E., Topal, T., 2005. Landslide susceptibility mapping: a comparison of logistic regression and neural networks methods in a moderate scale study, Hendek region (Turkey). Eng. Geol. 79, 251–266.

Zeverbergen, L.W., Thorne, C.R., 1987. Quantitative analysis of land surface topography. Earth Surf. Process. Landf. 12 (47–56), 1987.